# Nitrogen/Palladium-Codoped TiO$_2$ for Efficient Visible Light Photocatalytic Dye Degradation

Alex T. Kuvarega,[†] Rui W. M. Krause,*[,†,‡] and Bhekie B. Mamba[†]

[†]UJ Centre for Nanomaterials Science, Department of Chemical Technology, University of Johannesburg, P.O. Box 17011, Doornfontein, 2028, Johannesburg, South Africa

[‡]DST/NRF Centre of Excellence in Strong Materials, University of the Witwatersrand, Private Bag 3, Wits, 2050, Johannesburg, South Africa

ABSTRACT: Elimination of toxic organic compounds from wastewater is currently one of the most important subjects in water pollution control. Eosin Yellow, an anionic xanthene fluorescent dye, known to be carcinogenic, originates mainly from textile industrial processes and is resistant to conventional chemical or biological water treatment methods. Photocatalysis using non metal/platinum group metal-codoped TiO$_2$ may provide effective means of removing such dyes from contaminated water. In this study, nitrogen/palladium-codoped TiO$_2$ photocatalysts were prepared by calcination of the hydrolysis product of titanium isopropoxide, Ti(OC$_3$H$_7$)$_4$, with aqueous ammonia. Samples were characterized by Fourier transform infrared spectroscopy (FTIR), Raman spectroscopy, thermogravimetric analysis (TGA), diffuse reflectance UV−vis spectrophotometry, X-ray diffraction (XRD), X-ray photoelectron spectroscopy (XPS), scanning electron microscopy (SEM), and transmission electron microscopy (TEM). Anatase phase particles of size range 10−20 nm were confirmed by XRD, Raman, TEM, and SEM analysis. Codoping imparted a red shift in the absorption edges of the materials. Codoped TiO$_2$ showed greater photocatalytic Eosin Yellow degradation efficiency compared to singly doped N−TiO$_2$ or Pd−TiO$_2$ under visible light irradiation. The highest initial reaction rate of 2.238×10^{-2} min^{-1} was observed for N/Pd−TiO$_2$ (0.8% Pd). The results demonstrated that the N/Pd-codoped TiO$_2$ (0.6% Pd) sample could completely degrade the dye in 3 h, while the commercial TiO$_2$, (Degussa P25) showed the lowest dye degradation efficiency.
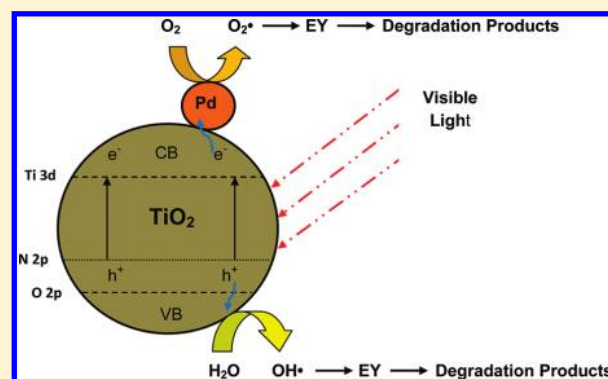
1. INTRODUCTION

In the past few years, there has been tremendous research and development in the area of photocatalysis. Photocatalysis using semiconductor particles has found increasing interest in solving global pollution problems. One of the major applications of this technology is the degradation of organic pollutants in water.[1] Compared to other semiconductor photocatalysts, titania (TiO$_2$) has so far been shown to be the most promising material used for both fundamental research and practical applications because of its high activity, good chemical inertness, safeness, nontoxicity, and low cost. However, pure TiO$_2$ is only active under ultraviolet (UV) light irradiation (E$_g$ = 3.2 eV), limiting its practical application in the visible region.[2]

Activation of TiO$_2$ is achieved through the absorption of radiation of ultra bandgap energy, resulting in the promotion of electrons from the valence band to the conduction band. This will create holes in the valence band. The holes can scavenge H$_2$O and OH molecules on the surface of the nanoparticle to form OH• radicals. The OH• radicals are highly oxidizing, attacking any organic compounds adsorbed onto the particle surface to form water and carbon dioxide. Electron−hole recombination is a major competitive deactivation process for this oxidation reaction.[3]

Several strategies have been attempted to improve the activity of TiO$_2$ in the visible region, including doping with other species.[4−7] Doping is the intentional introduction of impurities to the material for the purpose of modifying its electrical characteristics. An ideal dopant must increase the valence band edge, thus reducing the band gap without lowering the conduction band. It must also improve or minimize electron−hole recombination, so as to reduce any loss in quantum yield. Metals such as Fe, Mn, Cr, V, and Ni have been found to tune the electronic structure of TiO$_2$ and improve its photocatalytic activity in the visible range.[8] The positive effect of metal doping has been explained by the improved separation of electrons and holes on the surface of the photocatalyst. In most cases, however, the photoactivity of these doped samples is insufficient due to poor oxidative ability and low quantum efficiency as a result of an increase in the carrier recombination centers.[9] It has also been observed that some metals on TiO$_2$ surface can have no influence or even a detrimental effect on the photocatalytic degradation of investigated organic pollutants.[10] One conventional method for

preventing recombination is utilization of platinum group metal (pgm) catalysts, e.g., platinum, osmium, palladium, and rhodium, which are capable of collecting a large number of electrons and enhance the photoactivity by increasing the lifetime of holes. However, the use of noble metals as cocatalysts is a problem from the viewpoint of cost and availability.[11]

Anionic species such as nitrogen, carbon and sulfur were identified to potentially form new impurity levels close to the valence or conduction band of TiO_2, thereby lowering the band gap and shifting the absorption edge to the visible region. By far the most successfully synthesized and studied anion-doped TiO_2 is nitrogen-doped TiO_2. This is because nitrogen has a similar size to oxygen as well as low ionization energy. It is widely believed that the band gap of anatase TiO_2 might be narrowed as few crystal lattice oxygen atoms are substituted by nitrogen due to mixing of the N 2p orbital with O 2p orbital or creation of additional N 2p states within the bandgap of titania. It was also found that N concentration can significantly affect the mechanism of band structure changes. Band edge narrowing can possibly occur when doping levels reach a critical concentration. It was shown that the N 2p states hybridize with O 2p only when the N dopant concentration exceeds 20% in anatase TiO_2. Nitrogen-doped TiO_2 has been shown to exhibit higher photocatalytic activity under visible light irradiation.[12] However, there are still many controversies on the modification mechanism of TiO_2 doped with nitrogen.

More recently, the simultaneous doping of two kinds of atoms into TiO_2 has attracted considerable interest, since it could result in a higher photocatalytic activity and peculiar characteristics compared with single-element doping. Some studies on codoped TiO_2 with atoms such as C and N,[13] S and N,[14] F and N,[15] B and N,[16] C and S,[17] and N and a variety of metal ions[17−19] have been reported, and in some cases authors realized the synergistic effect of codoping. In a study by Cong et al., codoping of nitrogen and iron cations in TiO_2 led to the narrowing of the band gap and greatly improved photocatalytic activity in the visible region.[18] Wei et al. reported on codoping TiO_2 with lanthanum and nitrogen and observed a significant enhancement in the photodegradation of methyl orange under visible light. They suggested that the substitution of N for O was responsible for the band gap narrowing of TiO_2, and La doping reduced the aggregation of the powder in the preparation process.[19] Sun et al. observed that carbon and sulfur-codoped TiO_2 showed high photodegradation efficiency of 4-chlorophenol under visible light irradiation.[17] Yang and co-workers synthesized C-doped and C and V-codoped TiO_2 photocatalysts that were quite active for the degradation of acetaldehyde.[20]

Codoping approaches have shown that a second element confers a synergistic sensitizing effect to nonmetal-doped TiO_2, thereby enhancing visible light induced photoactivity. Wu et al.[21] reported enhanced visible-light photoactivity of palladium-modified nitrogen-doped TiO_2. They reported the formation of PdO nanoparticles on a PdO/TiON thin film that can be reduced to metallic palladium under visible light illumination, which may reduce the electron hole recombination rate during photocatalysis and enhance the visible light photoactivity. While codoping TiO_2 has achieved some results, there are still many misunderstandings on the modification mechanism due to widely varying experimental conditions, sample preparation techniques, determination of photoreactivity and the lack of detailed information about the effects of codoping on the electronic structure of TiO_2.[22]
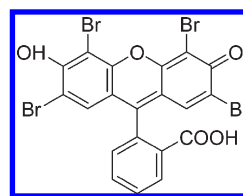

Figure 1. Chemical structure of EY.

Despite the development of effective visible light-induced photocatalysts in the past few decades, there have been only a limited number of reports on environmental applications of nonmetal/pgm-codoped TiO_2. The nonmetal/pgm codoping of TiO_2 may result in a material with excellent photocatalytic performance compared to singly doped TiO_2. In this work, nitrogen/palladium-codoped TiO_2 nanoparticle photocatalysts were synthesized by a modified sol−gel method and investigated for their visible light-induced photocatalytic degradation effect on Eosin Yellow (EY) (Figure 1). Among the different synthesis methods, the sol−gel method is the simplest and most economical, with capabilities of altering synthesis conditions without detrimental effects on the final product. The results demonstrated that codoping has strong effects on the optical and photocatalytic properties of the nanoparticle photocatalysts. N/Pd-codoped TiO_2 photocatalysts showed superior photocatalytic activity to N-doped TiO_2 but only over a narrow range of palladium concentrations. Beyond this range, the addition of Pd had an adverse effect on the visible light-induced degradation of EY. Thus, within a narrow composition range, a N/Pd-codoped TiO_2 nanoparticle photocatalyst has considerable potential to exert a photodegradation effect on organic dyes.

2. EXPERIMENTAL DETAILS

2.1. Preparation of Materials. N/Pd-codoped TiO_2 was prepared by a modified sol−gel method using ammonium hydroxide as a source of nitrogen, solvent for the Pd precursor, and a hydrolyzing reagent. A 10 mL portion of titanium isopropoxide, $Ti(OC_3H_7)_4$ (97%, Sigma Aldrich, Germany), was added to 50 mL of 2-propanol, C_3H_8O, (99.8%, Sigma Aldrich, Germany) and stirred for about 10 min. An appropriate amount of palladium diammine dichloride, $Pd(NH_3)_2Cl_2$, (45% Pd, PGM Chemicals, RSA) to give Pd:Ti proportions of 0.2%, 0.4%, 0.6%, 0.8% and 1.0%, was dissolved in 3 mL of 25% ammonia, NH_3, (Merck, Germany). The ammoniacal solution was then slowly added to the isopropoxide/propanol solution with vigorous stirring for about half an hour. Stirring was continued for 1 h. The resulting sol was dried in air at 80 °C for 12 h to obtain a white powder. The powder was calcined for 2 h at 500 °C in air in an electric furnace and characterized by various methods. The 0% Pd sample was prepared by the same method without the addition of Pd-$(NH_3)_2Cl_2$.

2.2. Characterization. Fourier transform infrared (FTIR) spectra were obtained on a Perkin-Elmer (FT-IR Spectrum 100) spectrophotometer using 4 cm^{-1} resolution and averaging 60 scans. Samples were analyzed in their powder form using a diamond/ZnSe universal attenuated total reflectance sample accessory.

Raman spectra were recorded on a Czerny-Turner micro-Raman spectrometer (Perkin-Elmer Raman microscope) equipped with a cooled charged coupled device (CCD) detector set at −50 °C and an Olympus microscope. Signals were obtained on
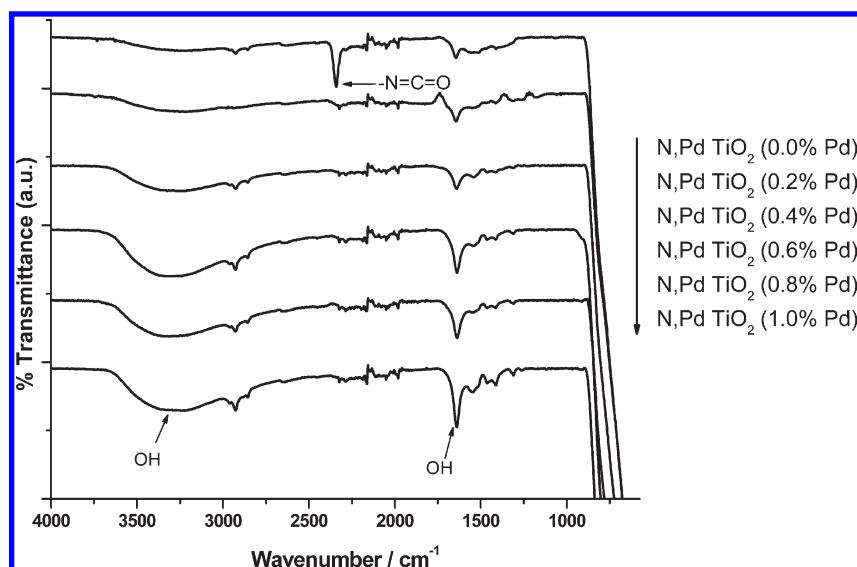
Figure 2. FTIR spectra of N/Pd-codoped TiO_2 with different palladium concentrations.

excitation of the samples by a red diode laser (785 nm). Measurements were done with the beam path set at 50X and an exposure time of 15 s.

X-ray diffraction (XRD) measurements were performed using an X-ray diffractometer (Philips PANanalytical X'pert) working at 40 kV and 40 mA. The Cu $K\alpha$ radiation ($\lambda = 0.15406$ nm), Ni filtered (0.02 mm) and masked (11.6 mm), was collimated with Soller slits (0.04 rad). Measurements were performed in the range $20-80°$ (2θ). Samples in their powder form were mounted on a Si sample holder using a bracket sample stage. Data analysis was performed using X'pert data collector software. The crystallite sizes were estimated by applying the Scherrer equation to the fwhm of the (101) peak of the anatase phase.

Optical properties were investigated using diffuse reflectance UV−vis absorption spectrophotometry on a Shimadzu UV - 2540 (Japan) equipped with an IRS 240 integrating sphere attachment. $BaSO_4$ was used as the reflectance standard.

Scanning electron microscopy (SEM) studies were carried out with an FEI Quanta Sirion microscope to observe the surface morphology of the powders after calcination. Surface elemental composition was analyzed using an energy dispersive X-ray spectrometer (EDX) attached to the SEM.

Transmission electron microscopy (TEM) analysis was performed under bright field on a Tecnai G^2 Spirit to observe the surface morphology, structure, and grain size of the nanoparticles.

Thermogravimetric analysis (TGA) was performed on a Perkin-Elmer Pyris thermal analyzer at a heating rate of 10 °C/min in nitrogen flow over a range of 30 °C − 900 °C in order to obtain thermal stability data.

X-ray photoelectron (XPS) surface elemental analysis was performed on a Physical Electronics (Quantum2000) spectrometer with Al kα (1486 eV) as the excitation source. The instrument was set to an X-ray power of 30 W, 100 μm beam diameter, 117.4 eV pass energy (wide), 29.35 eV pass energy (narrow) and a takeoff angle of 45°. XPS spectra of N 1s, O 1s, Pd 3d and Ti 2p were recorded. The binding energy was referenced to C 1s line at 284.76 eV for calibration. The atomic concentrations of these elements were obtained by comparing the peak areas of their spectra.

2.3. Evaluation of Photocatalytic Activity. The photocatalytic performance of the N/Pd-codoped TiO_2 (0.0 − 1.0% Pd)

was quantified by measuring the rate of degradation of EY under visible light irradiation. The catalyst (0.1 g) was suspended in 100 mL of EY solution (15 ppm) under visible light irradiation. A 150 W tungsten filament lamp (Eurolux), kept at a distance of 10 cm from the reaction vessel, was employed as a source of radiation. Prior to photocatalytic reactions, the suspensions were magnetically stirred in the dark for an hour to allow for adsorption equilibrium. The EY concentration became constant after about 40 min; therefore all suspensions were stirred for an hour in the dark to ensure adsorption equilibrium before illumination. Three milliliter aliquots of the suspension were withdrawn using a 6 mL Neomedic disposable syringe and filtered through a 0.2 μm Pall Acrodisc PSF membrane filter at 10 min intervals for 180 min. Variations in the concentration of EY under illumination were monitored using a Shimadzu UV-2450 spectrophotometer at $\lambda = 515$ nm. Commercial TiO_2 (Degussa P25) was used for comparison.

3. RESULTS AND DISCUSSION

FTIR studies were performed in order to determine the presence of functional groups as well as to study the surface changes on the particles at different Pd dopant levels (Figure 2). The presence of OH groups and water on the surface of the particles is evidenced by the appearance of a broad band between 3400 cm^{-1} and 3210 cm^{-1} for all samples. Another peak associated with O−H bending also appears around 1644 cm^{-1}. There is an increase in the intensity of the O−H peaks with increasing amount of Pd, showing the increase in surface OH groups. A highly intense peak centered around 520 cm^{-1} appears for all samples. This peak is attributed to the Ti−O bond. The peak at around 2340 cm^{-1}, which appears only for the N-doped sample, may be due to out of phase stretching of the −N═C═O bond. The peak disappears with the introduction of Pd due to the preferential formation of PdO enhanced by heat treatment in air.

Raman analysis of the samples was carried out on a Perkin-Elmer Raman microscope in the $100-800$ cm^{-1} frequency range with a 785 nm exciting line (Figure 3). Anatase TiO_2 shows six Raman active fundamental modes at 144 cm^{-1} (E_g), 197 cm^{-1} (E_g), 397 cm^{-1} (B_{1g}), 518 cm^{-1} ($A_{1g} + B_{1g}$) and 640 cm^{-1} (E_g).[7]
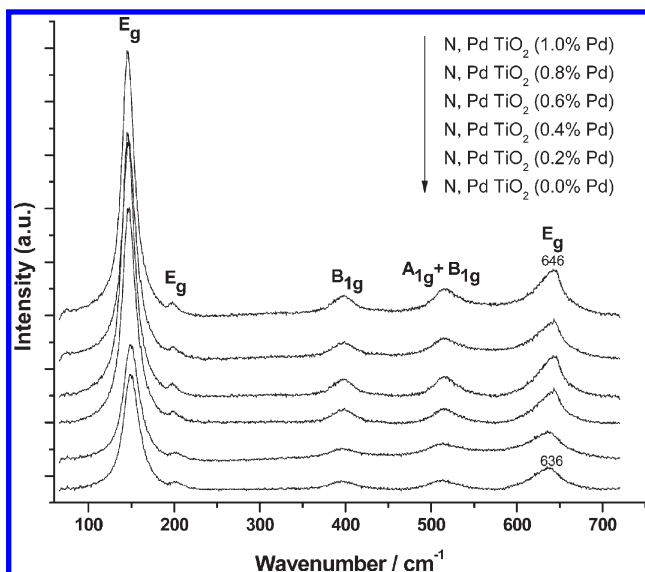
Figure 3. Raman spectra of N/Pd-codoped TiO$_2$ with different palladium concentrations.
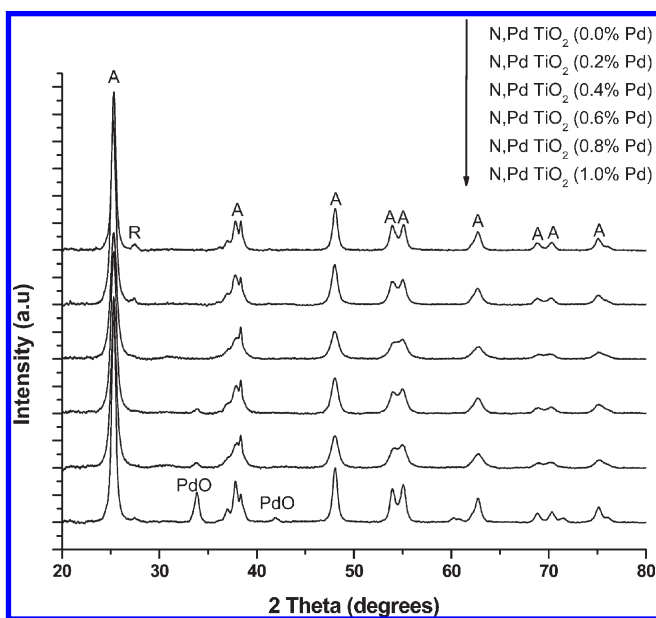

Figure 4. XRD patterns of N/Pd-codoped TiO$_2$ with different palladium concentrations (A = anatase).

Well-resolved Raman peaks were observed at 146 (E$_g$), 198 (E$_g$), 397 (B$_{1g}$), 516 (A$_{1g}$ + B$_{1g}$) and 636 (E$_g$) cm^{-1} in the spectra of all the samples calcined at 500 °C indicating that anatase was the predominant phase.

PdO has two Raman active modes (B$_{1g}$ + E$_g$). The allowed Raman modes are assigned to lines at 651 cm^{-1} (B$_{1g}$) and 445 cm^{-1} (E$_g$) respectively. The highly intense B$_{1g}$ mode is due to scattering from the (001) face and the Eg mode from the (110) face.[23] There is a shift in the position of the high frequency anatase E$_g$ with increasing amount of Pd, with the N/Pd-TiO$_2$ (0.0% Pd) appearing at 636 cm^{-1} while that of N/Pd-TiO$_2$ (1.0% Pd) appeared at 646 cm^{-1}. This shift may indicate the presence of PdO in high Pd level samples. No Raman lines due to PdO E$_g$ mode appeared in all the samples due to the low

Table 1. Effect of Pd Dopant Level on Average Particle Size and Phase Composition

sample	particle size (nm)	phase content (% anatase)
N/Pd-codoped TiO$_2$ (0.0% Pd)	17.5	95.6
N/Pd-codoped TiO$_2$ (0.2% Pd)	15.3	97.2
N/Pd-codoped TiO$_2$ (0.4% Pd)	16.9	98.4
N/Pd-codoped TiO$_2$ (0.6% Pd)	17.5	100.0
N/Pd-codoped TiO$_2$ (0.8% Pd)	15.7	100.0
N/Pd-codoped TiO$_2$ (1.0% Pd)	19.7	100.0

intensity, confirming the presence of the dopant in low concentrations on the crystal lattice. Sharp, narrow intense peaks at low wavenumbers confirmed the presence of the particles in the crystalline state. The TiO$_2$ crystalline structure was not changed by the doping procedure.

Figure 4 shows XRD patterns of the N-doped and N/Pd-codoped TiO$_2$ subjected to heat treatment at 500 °C for 2 h. Post synthesis treatment by thermal annealing resulted in increased crystallinity with anatase as the principal phase in agreement with Raman spectra. Peaks at 2θ values of 25.3, 37.6, 48.2, 53.9, 54.8, 62.7, and 75.2 corresponding to the (101), (004), (200), (105), (211), (204), and (215) planes, respectively, are all anatase signature peaks. Calcination resulted in intense and sharp anatase peaks. This is clearly indicative of an improvement in the degree of crystallinity corresponding to the formation of larger particles with fewer defects. No obvious diffraction peaks attributed to the N or Pd dopants were observed at low dopant levels. However, a PdO peak (101) at a 2θ value of 33.8 appears at Pd levels greater than 0.4%. Another PdO peak can be observed for the 1% Pd sample at a 2θ value of about 42. The absence of nitrogen or nitrogen-related compound XRD peaks could be explained by the low nitrogen dopant levels, or it could be an indication that the nitrogen atoms were well-dispersed in/on the TiO$_2$ particles. This resulted in the TiO$_2$ maintaining its anatase polymorph.

In N-doped TiO$_2$, the nitrogen atoms can substitute the O atoms in the lattice because of the similarity in the atomic radii of the two atoms. Pd will most likely be located in interstitial positions on the lattice rather than directly on Ti^{4+} sites because of the relatively large size difference between the ions (0.86 Å for Pd^{2+} and 0.68 Å for Ti^{4+}).[24]

The presence of Pd ions inhibited the anatase-to-rutile transformation as shown by the increase in the anatase phase with increasing Pd content (Table 1). This is ascribed to the fact that defects are formed on the grain boundaries of the TiO$_2$ resulting in distortion of ordering, consequently reducing the anatase-to-rutile transformation.

The crystallite size was calculated by X-ray line broadening analysis using the Scherrer equation:

$$D = \frac{k\lambda}{\beta \cos \theta}$$

where D is crystallite particle size, k is a constant of 0.9, λ is the wavelength (nm) of characteristic X-ray applied, β is the full width at half-maximum (fwhm) of the anatase (101) peak obtained by XRD, and θ is the Bragg angle.[25] Results of the particle sizes and phase composition are shown in Table 1. There is generally a slight increase in particle size with increasing amount of Pd. This can be attributed to the increase in crystallinity, which results in larger particles. Pd can occupy the interstitial positions on the
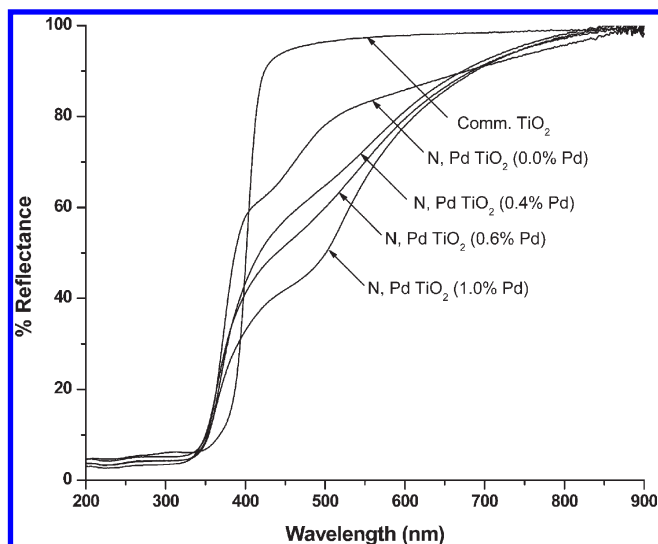
22113

dx.doi.org/10.1021/jp203754j |J. Phys. Chem. C 2011, 115, 22110–22120

Figure 5. Diffuse reflectance UV−vis spectra of N/Pd-codoped TiO$_2$ with different palladium concentrations.
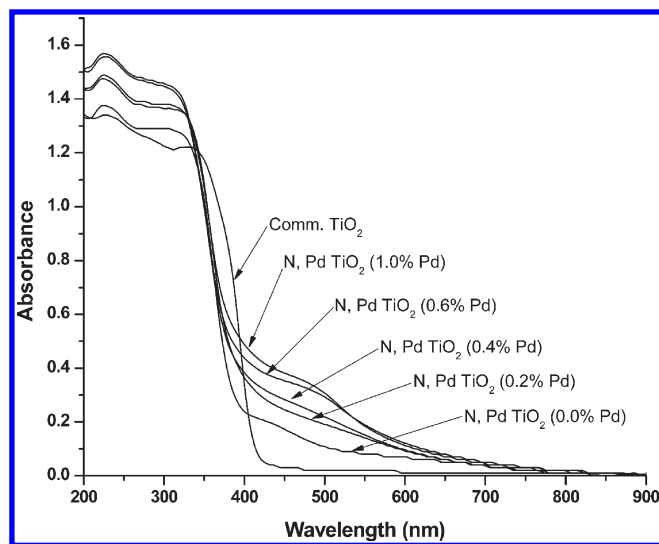

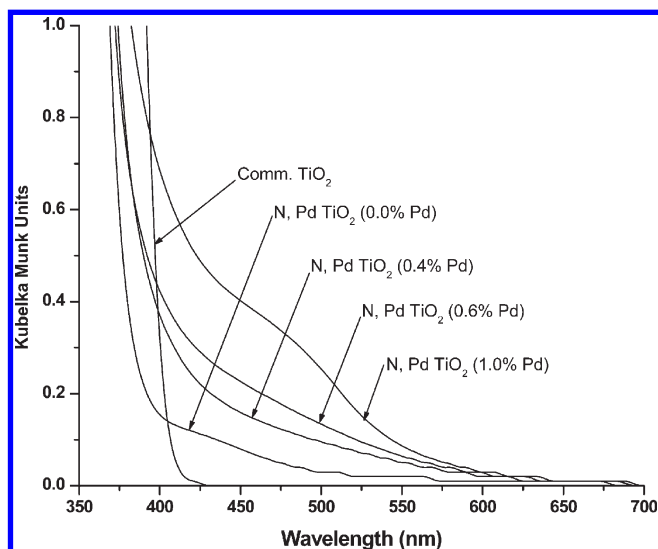**Figure 7.** UV−vis absorption spectra of N/Pd-codoped TiO$_2$ with different palladium concentrations.

Figure 6. Kubelka−Munk plots of N/Pd-codoped TiO$_2$ with different palladium concentrations.

Figure 8. Tauc plots of N/Pd-codoped TiO$_2$ with different palladium concentrations.

N-doped TiO$_2$ resulting in an increase in particle size with increasing amount of Pd. Maicu et al. reported on a particle size of 17 nm for Pd-doped TiO$_2$ (1.5% Pd) using the Scherrer equation.[26]

The phase content of TiO$_2$ samples can be calculated using the formula

$$X_A = \frac{1}{1 + \dfrac{I_R}{0.79 \cdot I_A}}$$

where X_A is the content of anatase, and I_A and I_R are integrated intensities of the anatase (101) and rutile (110) peaks respectively.[27] All the samples consisted of mainly the anatase phase.

Figure 5 shows the UV−vis diffuse reflectance spectra of the photocatalysts. The absorption edges of the N-doped and N/Pd-codoped samples were shifted to a longer wavelength region as
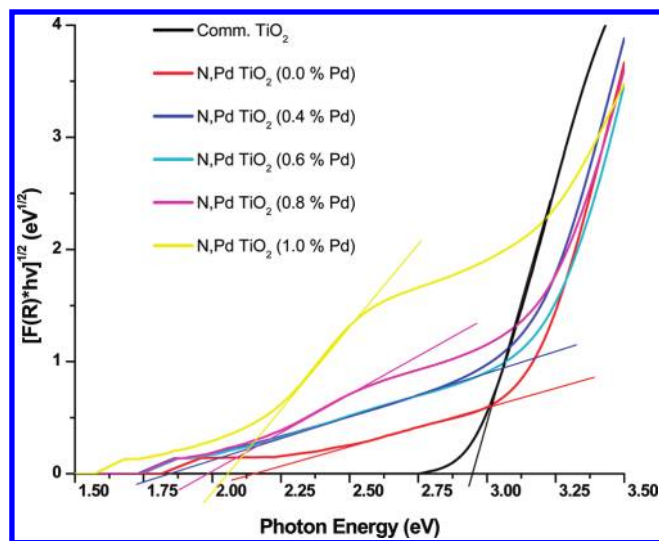
compared to that of commercial TiO$_2$. The shift in absorption intensity at wavelengths longer than 400 nm was enhanced with an increasing amount of Pd.[6] A broad band between 450 and 550 nm centered at 500 nm was observed in the absorption spectrum of N/Pd-codoped TiO$_2$ containing 1.0% Pd, owing to d−d transitions of PdO particles,[28] corresponding to the brown color of the powders. The spectrum of P25 showed single intense absorption around 400 nm due to a charge transfer transition between the lattice oxygen ligands (O^{2-}) and a central titanium ion (Ti^{4+}).[24] It can be seen that the N, Pd TiO$_2$ (0.0% Pd) sample presents a significant absorption in the visible region between 400 and 700 nm. This could be due to the excitation of electrons from localized nitrogen 2p levels in the band gap to the vacant CB, confirming the presence of Ti−N bonds.[18] Qui et al. reported that N doping, even with significantly high doping levels, may not cause significant band gap narrowing effects.[29] The major effect of N doping on the absorption spectra is the greatly
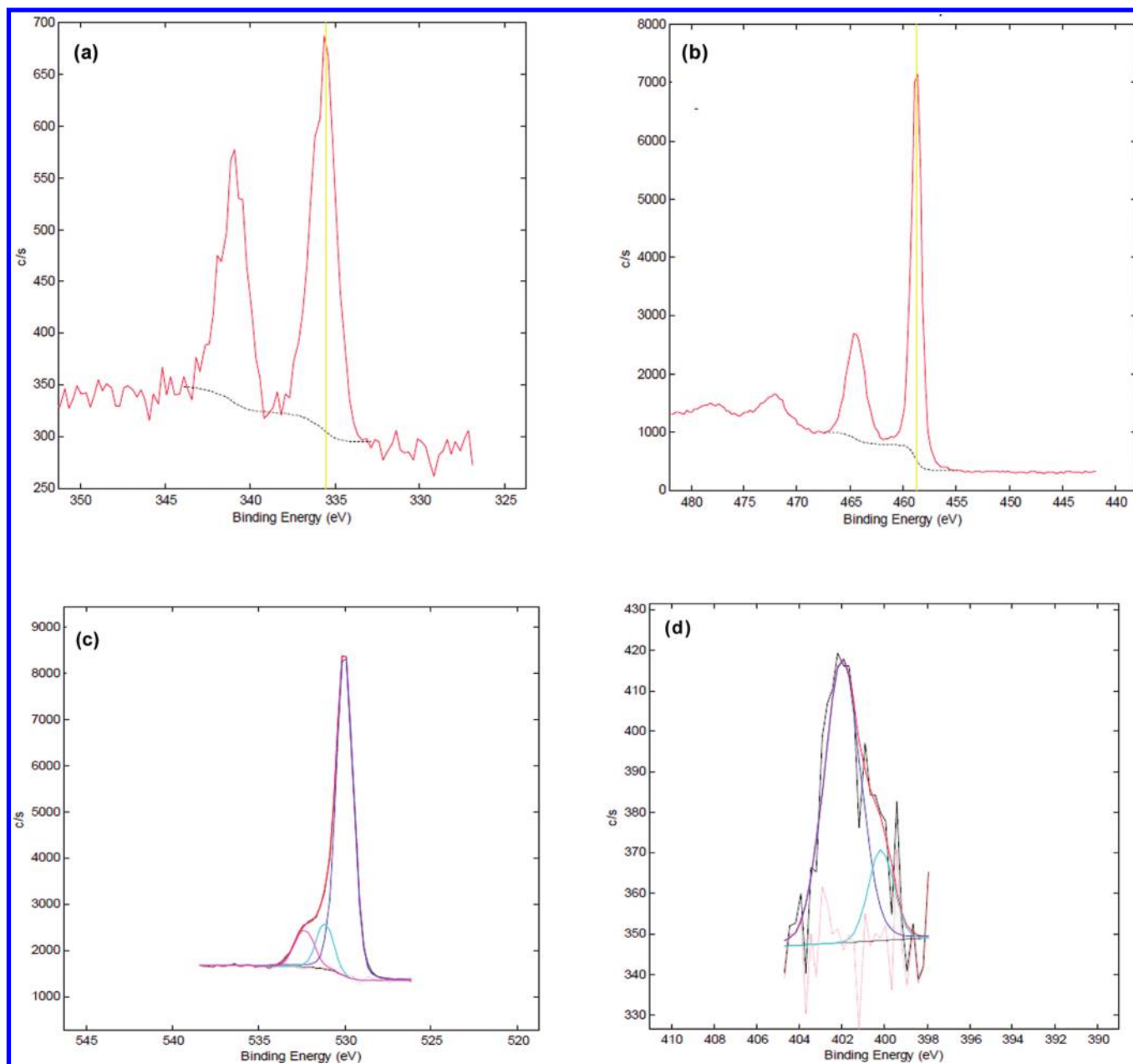
Table 2. Effect of Pd Dopant Level on Band Gap

sample	indirect band gap (eV)
commercial TiO_2 (Degussa P25)	2.95
N/Pd-codoped TiO_2 (0.0% Pd)	2.16
N/Pd-codoped TiO_2 (0.4% Pd)	1.87
N/Pd-codoped TiO_2 (0.6% Pd)	1.85
N/Pd-codoped TiO_2 (0.8% Pd)	1.99
N/Pd-codoped TiO_2 (1.0% Pd)	2.06

Figure 9. SEM image (a), TEM images (b,c), and EDX spectrum (d) of N/Pd-codoped TiO_2 (0.6% Pd).

Figure 10. TGA curves of N/Pd-codoped TiO_2 with different palladium concentrations.

Figure 11. XPS survey scan of (a) N/Pd-codoped TiO_2 (0.6% Pd) and (b) N-doped TiO_2.

enhanced absorption at long wavelength regions (>400 nm) in the N-doped TiO_2, which might be useful in enhancing the photocatalytic visible light activities of these materials. An increasing amount of Pd led to higher absorbencies in the visible region, emphasizing the synergistic effect of codoping in enhancing visible light activity.

The diffuse reflectance spectra were plotted as the Kubelka—Munk function, $F(R)$, versus wavelength based on the Kubelka—Munk equation:

$$F(R) = \frac{(1-R)^2}{2R}$$

where reflectance, $R = R_{sample}/R_{reference}$ (Figure 6). The plot shows a red shift in the absorption coefficient of the doped photocatalyst. For a semiconductor material, the Kubelka—Munk function allows the construction of a Tauc Plot: $[F(R) \cdot h\nu]^n$ versus $h\nu$. The type of transition in TiO_2 is not clear.[30] For a

Figure 12. High-resolution XPS scan over (a) Pd 3d, (b) Ti 2p, (c) O 1s in N/Pd-TiO$_2$, and (d) N 1s in N-TiO$_2$.

direct allowed band gap semiconductor, the plot with $n = ^1/_2$ will show a linear Tauc region just above the optical absorption edge. Extrapolation of this line to the photon energy axis yields the semiconductor band gap, a key indicator of its light harvesting efficiency under solar illumination. Indirect allowed band gap materials show a Tauc region with $n = 2$.[31]

Comparison of the spectra of commercial and codoped samples show no notable differences in the UV region, with the strong, broad absorption observed below 400 nm associated with charge-transfer from the valence to the conduction band of the TiO$_2$.[26] As the palladium doping amount is increased, band tailing becomes evident, with the onset of absorption at lower energy. The doping smears out the linear region, making a more rounded shape (Figure 7).

The character of the bandgap may become more indirect with added palladium. The red-shift in the absorption edges are typically attributed to the sp−d exchange between the TiO$_2$ band electrons and localized d-electrons associated with the doped Pd ions. The absorption at low energy in higher dopant samples may indicate the formation of palladium-derived states near the band edge. Band tails can arise from perturbations in the band structure caused by impurities and disorder. States introduced by impurities overlap at high concentrations and evolve into impurity bands. The tails' intensity increases with increasing palladium levels. The tails are most likely related to the increase of impurity states.[32] Therefore, the low-energy absorption onset is likely an electron transition from the valence band to palladium-derived impurity states.

The band gaps (Eg) for all the catalysts were determined from the extrapolation of the linear fit for the Tauc plot onto the low energy axis (Figure 8).[33] Commercial TiO$_2$ shows a well-defined

22116

dx.doi.org/10.1021/jp203754j |*J. Phys. Chem. C* 2011, 115, 22110–22120

Table 3. Core-Level XPS Elemental Analysis Results for the N-Doped TiO_2 and N/Pd-Codoped TiO_2

	atomic percentages				
sample	Ti	O	Pd	N	C
N-doped TiO_2	20.8	56.9		1.6	18.6
N/Pd-codoped TiO_2	21.1	59.5	0.8		14.8

absorption edge that can be fit reliably to the energy axis. Assuming an indirect allowed band gap for all the samples, there is generally a gradual reduction in band gap with increasing amount of Pd. However at much higher Pd content (1.0%), the band gap increases due to the dominance of the d−d transitions over the sp−d transitions (Table 2). This might also be due to the preferential formation of PdO at higher Pd levels, confirmed by XRD.

SEM image of one of the thermally treated N/Pd-codoped TiO_2 samples is shown below (Figure 9a). The sample consists of small, nearly spherical and larger elongated particles. The size of the particles is in the nanometer range. The particles show some degree of aggregation. TEM images confirm the presence of Pd deposits on the surface of the N-doped TiO_2 (Figure 9b and 9c). Pd deposits are well dispersed on many of the TiO_2 particles and had the diameters predominantly ranging from 1 to 2 nm. The size of the TiO_2 particles is approximately in the range of 15−20 nm, consistent with XRD measurements. This is in agreement with results reported by Wu et al.[34]

The elemental composition of the various samples was estimated by EDX. The EDX spectra of the codoped TiO_2 show signals directly related to the dopants (Figure 9d). The spectrum indicates that the main components are O and Ti with low levels of Pd. This confirms the formation of N/Pd-codoped TiO_2. Low intensity peaks due to Pd, a codopant, are also visible. C was used as the tape, so the C peak also appears on the EDX spectrum.

Figure 10 shows the thermogram obtained for some N/Pd-codoped TiO_2 heated at 500 °C. The mass loss around 100 °C is attributed to the loss of water adsorbed onto the particle surface. A small weight loss from 100 °C up to about 900 °C could be due to loss of nitrogen or carbon related materials entrapped within the nanoparticles. The total mass loss of between 2.0% and 5.5% shows the exceptionally high thermal stability of the materials. This confirms that much of the nitrogen and carbon material was lost through calcination at 500 °C.

The surface compositions of the catalysts were confirmed by XPS analysis. Samples were analyzed without any sputtering using an instrument with a detection limit of 0.1 atom %. Figure 11 shows representative XPS survey spectra of N/Pd-codoped TiO_2 (0.6% Pd) (a) and N-doped TiO_2 powders (b). Photoelectron peaks of Ti 2p and O 1s are clearly visible for both samples. In Figure 11a, the presence of Pd in the N/Pd-codoped TiO_2 (0.6%) sample was confirmed by the appearance of Pd 3d and Pd 3s peaks. A B 1s peak appeared in both samples and can be attributed to impurities from the glass reaction vessel used in preparing the samples. S was also detected in the N-doped sample.

No observable N 1s photoelectron peaks appeared for N/Pd-codoped TiO_2 (0.6% Pd) due to the low levels of doped nitrogen after calcination at 500 °C, or the peaks could have been below the detection limit of the instrument. It is also possible that the Pd could be sitting on the N defects sites on the TiO_2 particles,
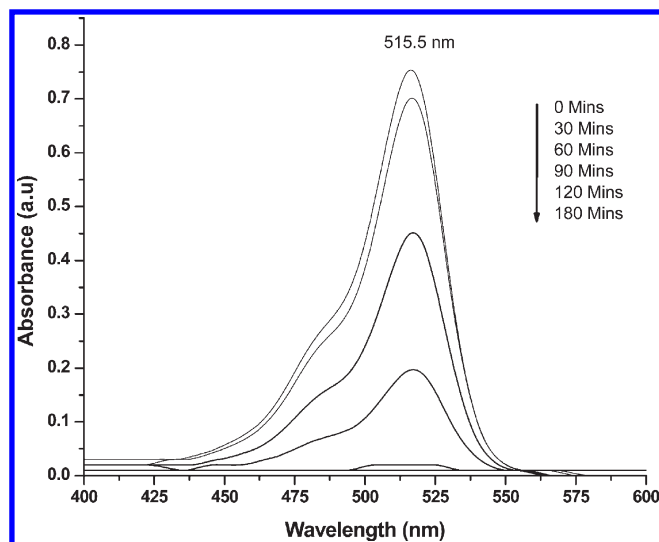
Figure 13. EY degradation profile using N/Pd-TiO_2 (0.6% Pd).

Table 4. Percentage Degradation after Exposure to Visible Radiation

sample	% degradation after 180 minutes
commercial TiO_2 (Degussa P25)	18.2
N/Pd-codoped TiO_2 (0.0% Pd)	44.0
N/Pd-codoped TiO_2 (0.4% Pd)	95.7
N/Pd-codoped TiO_2 (0.6% Pd)	100.0
N/Pd-codoped TiO_2 (0.8% Pd)	92.5
N/Pd-codoped TiO_2 (1.0% Pd)	65.8

thereby reducing the chances of emission from N. Samples were not argon sputtered for surface cleaning prior to analysis. This might have caused poor emission from the N1s due to superficial contaminants.

Figure 12 shows the high-resolution XPS scans over the Pd 3d, Ti 2p, O 1s, and N 1s peak regions. The binding energies of Pd $3d_{5/2}$ (335.6 eV) and $3d_{3/2}$ (341.6 eV) revealed that palladium was in the form of PdO or metallic Pd for N/Pd-codoped TiO_2.[6] Loaded Pd was oxidized to PdO in the preparation procedure in agreement with Raman, SEM, and XRD observations. Another peak at around 671.2 eV (Pd 3s) signals the presence of a small amount of Pd^0 in the codoped samples. Two peaks around 458.3 and 464.3 eV were observed for both samples. These peaks can be assigned to the spin orbit doublet of Ti $2p_{3/2}$ and Ti $2p_{1/2}$, respectively, indicating the presence of TiO_2. This is in agreement with Raman and XRD results. Other peaks associated with Ti were observed at about 37.5 eV (Ti 3p), 61.0 eV (Ti 3s), and 561.0 eV (Ti 2s) (Figure11). The peak at 37.5 eV confirmed the presence of Ti^{4+} as an oxide, while the one at 61.0 eV could possibly be due to the presence of Ti^{3+} again in the oxide form, indicating the possible formation of oxygen vacancies (defects) on the TiO_2 surface. The peak at 530.2 eV for both samples is attributed to the O^{2-} ion (O $1s_{1/2}$) in the TiO_2 lattice or PdO. This peak shows a shoulder that stretches up to about 335.0 eV. This shoulder could be due to OH groups from Ti−OH bonds. The presence of N in the N-doped TiO_2 was confirmed by the appearance of a N 1s peak around 400 eV (Figure 12d). Asahi and co-workers reported three N 1s peaks with binding energies
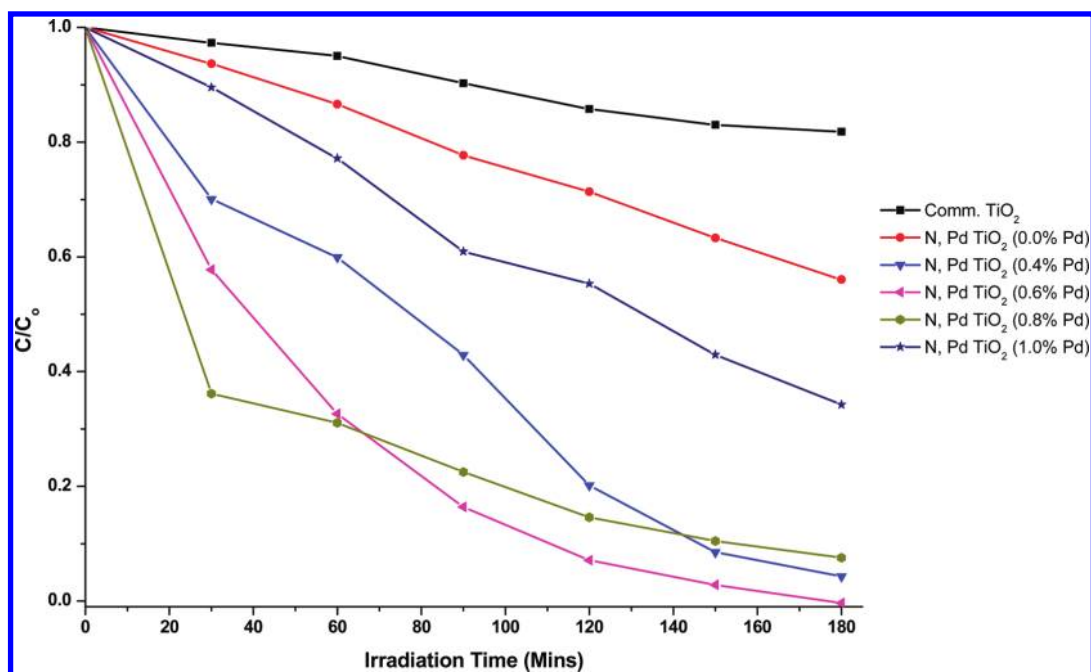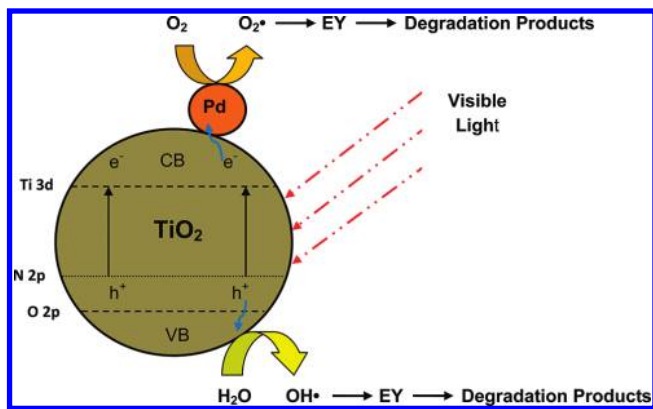
22117

dx.doi.org/10.1021/jp203754j |*J. Phys. Chem. C* 2011, 115, 22110–22120

Figure 14. EY degradation efficiency by various photocatalysts.

Scheme 1. Proposed Visible Light Induced Photocatalytic Mechanism of N/Pd-Codoped TiO$_2$ Photocatalyst

of 402, 400, and 396 eV, which were assigned as atomic β-N (396 eV) and molecularly chemisorbed γ-N$_2$ (400 and 402 eV).[5] This could also indicate the presence of NO species since the N 1s is attributed to NH$_3$ or NOx species.[35] The presence of Ti−N bonds cannot be ruled out. The N in this bond is also expected to appear in the same region.

Table 3 shows the atomic relative element composition of the materials from XPS scans over N 1s, O 1s, Pd 3d, and Ti 2p spectral regions for both samples. There are very small differences in the amount of Ti and O in the samples. However, introduction of Pd appeared to lower the nitrogen content. Amount of Pd in the codoped sample was within the expected range for the sample.

3.1. Dye Degradation. The amount of EY was plotted as a function of irradiation time. It is clear, that the photodegradation of EY in the presence of the semiconductor powders led to the disappearance of the compound (Figure 13). The disappearance

of the 515 nm absorption band suggests the chromophore responsible for the characteristic color of the dye was being broken down. Complete dye degradation was realized after 180 min for the N/Pd-TiO$_2$ (0.6% Pd) sample.

The apparent rate constants obtained with various catalyst samples with different palladium contents are shown in Table 4. The degradation rate of EY on the commercial TiO$_2$ under visible light irradiation is very low (18.2%). After 3 h of illumination, no detectable decolorization was observed for the commercial TiO$_2$. By contrast, N-doped and N/Pd-codoped TiO$_2$ nanostructures exhibited substantial photocatalytic activity within the time frame of the tests. Recent research shows that the desired band gap narrowing of TiO$_2$ can be better achieved by using nonmetal elements such as N.[36] Liu et al.[37] prepared N-doped TiO$_2$ by using titanium isopropoxide and ammonia as precursors. 10 mg/L of the calcined photocatalyst was tested for the degradation of 15 mL of 0.03 mM Acid Orange 7 (AO7), procion red MX-5B, and Reactive Black 5 (RB5) under sun light irradiation. They observed 70% degradation of AO7 in 1 h, 100% degradation of MX-5B in 3 h, and 80% total organic carbon (TOC) removal in RB5 in 4 h.

The higher photocatalytic activity observed for N/Pd-co-doped TiO$_2$ (0.6% Pd) may be attributed to the Pd effectively capturing the photoinduced electrons, which inhibited their recombination with holes and improved the photocatalytic activity. It is believed that the metal induces greater enhancements in the photocatalytic activity of TiO$_2$ by creating a Schottky junction between metal and semiconductor. The metal particle acts as a sink for photogenerated electrons, reducing the rate of their recombination with holes.[26] There is an increase in the degradation efficiency with increasing Pd content up to 0.6% Pd then a decrease to 65.8% for the highest Pd content sample (Figure 14). A similar trend was reported for the oxidation of benzene using Pd-doped TiO$_2$.[38] The dosage level is an important factor in influencing the enhancement effect of noble metals. Below an
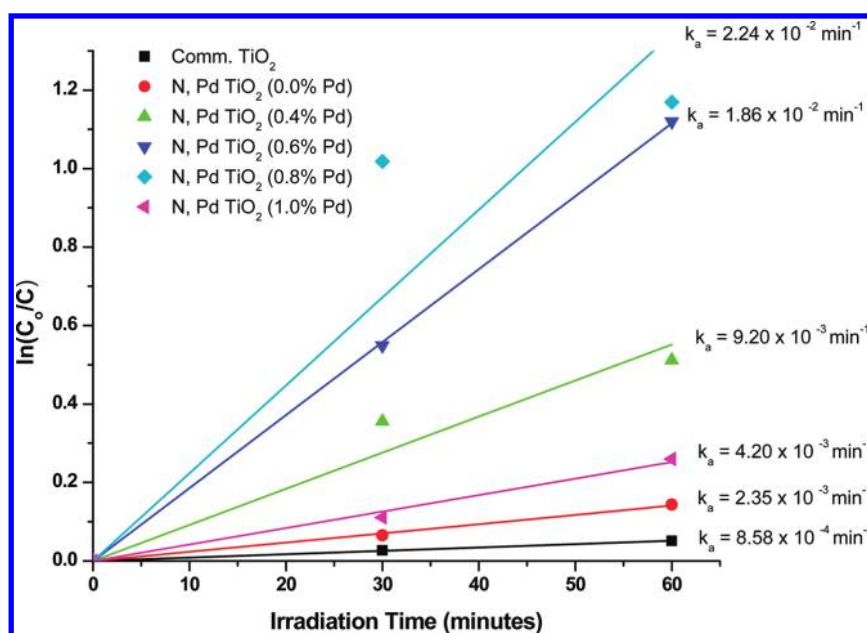
Figure 15. Kinetics of EY degradation in the first 60 min of visible light irradiation.

optimum dosage level, pgm's can act as electron—hole separation centers, improve the charge separation, and thus enhance the photocatalytic efficiency of modified TiO_2. However as dosage levels exceed optimum loading, they can act as electron—hole recombination centers, which are detrimental to the photocatalytic activity.[36] This may also be due to shading of the photosensitive surface of TiO_2 by the metal dopant. This observation led to the conclusion that the optimum amount of dopant for effective photoactivity is 0.6% Pd. Higher Pd levels (1.0%) led to lower photodegradation rates, as these become recombination centers, thus short circuiting the system.

Nitrogen and palladium have synergistic effects on improving the photocatalytic activity under visible light irradiation. Under visible light irradiation, substitutional nitrogen dopant can create intra bandgap states close to the valence band edges leading to a narrower band gap than P25 TiO_2. Scheme 1 shows the proposed possible mechanism for the synergistic effects of nitrogen and palladium on the codoped photocatalysts. Under UV light illumination, electrons (e^-) are excited from the valence band (VB) to the conduction band (CB), creating holes (h^+) in the valence band. Normally, these charge carriers quickly recombine, and only a fraction of the electrons and holes participate in the photocatalytic reaction, resulting in low reactivity. Introduction of substitutional or interstitial nitrogen in the TiO_2 will result in the formation of impurity states close to the valence band. This enhances the visible light activity of the nanoparticles as electrons can be excited from the nitrogen 2p orbitals to the conduction band.[5] In the presence of Pd, the photogenerated electrons are trapped, leading to electron—hole separation. The holes can scavenge surface adsorbed water or hydroxyl molecules generating highly reactive hydroxyl radical species. The electrons, on the other hand, scavenge the oxygen molecules to form very reactive superoxide radicals.[39] Both radicals are highly reactive toward the degradation of the organic compounds such as EY used in the present study.

Generally, the photodegradation reaction of organic compounds can be described by the Langmuir—Hinshelwood model, where the photocatalytic activity of the catalysts can be quantitatively evaluated by the equation

$$\ln C_0/C = kt$$

where k is the apparent reaction rate constant and C_0 and C represent the concentrations at the initial time and time t, respectively.[40]

The kinetics of EY degradation is presented in Figure 15 by plotting the logarithm of the normalized dye concentration against irradiation time for the first 60 min. Fairly good linear relationships were observed, indicating that all reactions followed first-order kinetics. Sun et al.[35] reported a k value of 1.6×10^{-3} min^{-1} for N-doped TiO_2 prepared at a pH of 5.5. This value is lower than the k value of 2.35×10^{-3} min^{-1} observed for N/Pd (0.0% Pd). N/Pd-codoped TiO_2 (0.8% Pd) showed the highest initial rate (2.238×10^{-2} min^{-1}), indicating faster dye decolorization and higher catalytic activity. However, the rate decreased after 60 min, probably due to pseudo-first-order kinetics. The initial rate for the N/Pd-codoped TiO_2 (0.8% Pd) was higher than that reported for Co-, Cu-, Os-, Pt-, Fe-, Cr-, V-, Ni-, Ru-, Ag-, Rb-, Y-, and La-doped TiO_2 for the degradation of methylene blue under visible light irradiation.[41] Li et al.[6] reported on the visible light activity of palladium-modified nitrogen-doped titanium oxide (TiON/PdO) nanoparticles synthesized by a sol—gel process for photocatalytic degradation of humic acid. They realized an increase in the reaction rate constant from 0.0002 min^{-1} for TiON to 0.0003 min^{-1} for TiON/PdO containing 0.5% PdO. When the palladium dopant concentration was further increased, an inverse effect was observed, wherein the rate constant decreased to 0.00015 min^{-1} for TiON/PdO with 2.0% PdO. These rates are several orders lower than the ones observed for the N/Pd-codoped TiO_2. The better performance of N/Pd-codoped nanoparticles could be explained by the synergistic effects of codoping a nonmetal and a pgm.

4. CONCLUSION

A simple method was developed for the preparation of highly visible active nanocrystalline N-doped and N/Pd-codoped TiO_2

photocatalysts by calcination of the hydrolysis product of titanium isopropoxide with ammonia solution. According to the XRD and Raman analysis, we found that the photocatalysts were crystalline and consisted of mainly the anatase phase of TiO_2. UV—vis spectra indicated that the nitrogen and nitrogen—palladium codoping causes the absorption edge of TiO_2 to shift to a lower energy region, evidenced by the reduction in the band gaps. Highest photocatalytic activity was observed for the N/Pd-codoped TiO_2 (0.6% Pd) sample. Undoped TiO_2 and P25 as well as N/Pd-codoped TiO_2 (1.0% Pd) showed the lowest degradation efficiency. Control of the dopant amount is very important, as higher levels may result in the dopants becoming recombination centers. The synergistic effects of N and Pd codoping led to enhanced utilization of solar energy through narrowing of the band gaps. The presence of Pd sufficiently promoted the separation of photogenerated holes and electrons by acting as electron traps leading to high photodegradation efficiency of EY under visible light irradiation.

■ AUTHOR INFORMATION

Corresponding Author
*E-mail: rkrause@uj.ac.za. Tel: (+2711) 559 6152. Fax: (+2711) 559 6425.

■ ACKNOWLEDGMENT

■ REFERENCES

(1) Malato, S.; Ibanez, P. F.; Maldonado, M. I.; Blanco, J.; Gernjak, W. *Catal. Today* **2009**, *147*, 1–59.

(2) Song, K.; Zhou, J.; Bao, J.; Feng, Y. *J. Am. Ceram. Soc.* **2008**, *91* (4), 1369–1371.

(3) Mills, A.; Hunte, S. L. *J. Photochem. Photobiol., A* **1997**, *108*, 1–35.

(4) Nosaka, Y.; Matsushita, M.; Nishino, J.; Nosaka, A. Y. *Sci. Technol. Adv. Mater.* **2005**, *6*, 143–148.

(5) Asahi, R.; Morikawa, T.; Ohwaki, T.; Aoki, K.; Taga, Y. *Science* **2001**, *293*, 269.

(6) Li, Q.; Xie, R.; Mintz, E. A.; Shang, J. K. *J. Am. Ceram. Soc.* **2007**, *90* (12), 3863–3868.

(7) Morikawa, T.; Ohwaki, T.; Suzuki, K.; Moribe, S.; Kubota, S. T. *Appl. Catal. B: Environ.* **2008**, *83*, 56–62.

(8) Wang, J.; Tafen, D. N.; Lewis, J. P.; Hong, Z.; Manivannan, A.; Zhi, M.; Li, M.; Wu, N. *J. Am. Chem. Soc.* **2009**, *131*, 12290–12297.

(9) Li, D.; Chen, Z.; Chen, Y.; Li, W.; Huang, H.; He, Y.; Fu, X. *Environ. Sci. Technol.* **2008**, *42*, 2130–2135.

(10) Sivalingam, G.; Nagaveni, K.; Hegde, M. S.; Madras, G. *Appl. Catal., B* **2003**, *45*, 23–38.

(11) Lee, S. K.; Mills, A. *Platinum Metals Rev.* **2003**, *41* (2), 61–72.

(12) Lin, Z.; Orlov, A.; Lambert, R. M.; Payne, M. C. *J. Phys. Chem. B* **2005**, *109*, 20948.

(13) Cong, Y.; Chen, F.; Zhang, J. L.; Anpo, M. *Chem. Lett.* **2006**, *35*, 800–801.

(14) Liu, H. Y.; Gao, L. *J. Am. Ceram. Soc.* **2004**, *87*, 1582–1584.

(15) Li, D.; Haneda, H.; Hishita, S.; Ohashi, N. *Chem. Mater.* **2005**, *17*, 2588–2595.

(16) In, S.; Orlov, A.; Berg, R.; Garcia, F.; Sergio, P. J.; Tikhov, M. S.; Dominic, S. W.; Lambert, R. M. *J. Am. Chem. Soc.* **2007**, *129*, 13790–13791.

(17) Sun, H.; Bai, Y.; Cheng, Y.; Jin, W.; Xu, N. *Ind. Eng. Chem. Res.* **2006**, *45*, 4971–4976.

(18) Cong, Y.; Zhang, J. L.; Chen, F.; Anpo, M.; He, D. *J. Phys. Chem. C* **2007**, *111*, 10618–10623.

(19) Wei, H.; Wu, Y.; Lun, N.; Zhao, F. *J. Mater. Sci.* **2004**, *39*, 1305–1308.

(20) Yang, X. X.; Cao, C.; Hohn, K.; Erickson, L.; Maghirang, R.; Hamal, D.; Klabunde, K. *J. Catal.* **2007**, *252*, 296–302.

(21) Wu, P.; Xie, R.; Imlay, J. A.; Shang, J. K. *Appl. Catal. B: Environmental* **2009**, *88*, 576–581.

(22) Gao, P.; Zhang, X.; Zhou, W.; Wu, J.; Liu, Q. *J. Semicond.* **2010**, *31* (3), 032001-1–032001-6, DOI: 10.1088/1674-4926/31/3/032001.

(23) McBride, J. R.; Hass, K. C.; Weber, W. H. *Phys. Rev. B* **1999**, *44* (10), 5016–5028.

(24) Shah, S. I.; Li, W.; Huang, C. P.; Jung, O. C. *Proc. Natl. Acad. Sci. U.S.A.* **2002**, *99* (9), 6482–6486.

(25) Yan, M. C.; Chen, F.; Zhang, J. L.; Anpo, M. *J. Phys. Chem. B* **2005**, *109*, 8673–8678.

(26) Maicu, M.; Hidalgo, M. C.; Colon, G.; Navio, J. A. *J. Photochem. Photobiol., A* **2011**, *217*, 275–283.

(27) Hirano, M.; Nakahara, C.; Ota, K.; Tanaike, O.; Inagaki, M. *J. Solid State Chem.* **2003**, *170*, 39–47.

(28) Zhang, Z.; Mestl, G.; Knozinger, H.; Sachtler, W. M. H. *Appl. Catal., A* **1992**, *89*, 155–168.

(29) Qiu, X.; Burda, C. *Chem. Phys.* **2007**, *339*, 1–10.

(30) Li, Q.; Xie, R.; Shangw, J. K. *J. Am. Ceram. Soc.* **2007**, *90* (4), 1045–1050.

(31) Serpone, N.; Lawless, D.; Khairutdinov, R. *J. Phys. Chem.* **1995**, *99*, 16646–16654.

(32) Kittilstved, K. R.; Liu, W. K.; Gamelin, D. R. *Nat. Mater.* **2006**, *5*, 291–297.

(33) Wu, Y.; Zhang, J.; Xiao, L.; Chen, F. *Appl. Surf. Sci.* **2010**, *256*, 4260–4268.

(34) Wu, Z.; Sheng, Z.; Liu, Y.; Wang, H.; Tang, N.; Wang, J. *J. Hazard. Mater.* **2009**, *164*, 542–548.

(35) Sun, H.; Bai, Y.; Liu, H.; Jin, W.; Xu, N.; Chen, G.; Xu, B. *J. Phys. Chem. C* **2008**, *112*, 13304–13309.

(36) Han, F.; Kambala, V. S. R.; Srinivasan, M.; Rajarathnam, D.; Naidu, R. *Appl. Catal., A: Gen.* **2009**, *359*, 25–40.

(37) Liu, Y.; Chen, X.; Li, J.; Burda, C. *Chemosphere* **2005**, *61*, 11–18.

(38) Zhong, J. B.; Lu, Y.; Jiang, W. D.; Meng, Q. M.; Xi Yang, He X. Y.; Li, J. Z.; Chen, Y. Q. *J. Hazard. Mater.* **2009**, *168*, 1632–1635.

(39) Yu, J.; Ma, T.; Liu, S. *Phys. Chem. Chem. Phys.* **2011**, *13*, 3491–3501.

(40) Xu, Y. J.; Zhuang, Y.; Fu, X. *J. Phys. Chem. C* **2010**, *114*, 2669–2676.

(41) Choi, J.; Park, H.; Hoffmann, M. R. *J. Phys. Chem. C* **2010**, *114*, 783–792.